Polymer Vol. 38 No. 24, pp. 6031–6047, 1997

0032-3861/97/$17.00 + 0.00

PII: S0032-3861(97)00161-4

Chain conformation and molecular packing in poly(*p*-oxybenzoate) single crystals at ambient temperature

J. Liu, B.-L. Yuan and P. H. Geil*
Department of Materials Science and Engineering and Materials Research Laboratory, University of Illinois, Urbana, IL 61801, USA

and D. L. Dorset
Hauptman-Woodward Medical Research Institute, 73 High Street, Buffalo, NY 14203, USA
(Received 22 July 1996; revised 27 January 1997)

The chain conformation and molecular packing of poly(*p*-oxybenzoate) (PpOBA) at room temperature have been determined using computer modelling and direct phasing based on electron diffraction data from lamellar and whisker single crystals. In the triclinic (metrically orthorhombic) phase I and orthorhombic phase II the unit cell parameters are $a = 7.45$, $b = 5.64$, $c = 12.47$ Å, $\alpha = \beta = \gamma = 90°$ for I and $a = 11.15$, $b = 3.80$ and $c = 12.56$ Å for II. The best agreement between the computer modelling and the experimental diffraction patterns suggests the carbonyl groups in Phase I are nearly parallel to the planes of the phenyl rings in the [001] projection, the two phenyl rings being at an angle of 124° with respect to each other along the *c*-axis. The two chains in the unit cell of these 'perfect' crystals have a parallel orientation and are staggered by ±0.14 Å along the *c*-axis from the positions they would have in the $Pbc2_1$ space group. In Phase II, space group $Pca2_1$ the conformation of the chain is nearly the same as in phase I (phenyl ring angle = *ca* 128°) and there is insufficient evidence to determine if chain stagger occurs. The results of the direct phasing are in good agreement, including the stagger in Phase I. Simulated X-ray diffraction scans are compared with measured scans for samples of various solution polymerization history and resulting morphology and phase composition. © 1997 Elsevier Science Ltd.

(Keywords: poly(*p*-oxybenzoate); crystal structure; electron diffraction)

INTRODUCTION

The crystal structure of poly(*p*-oxybenzoate) (PpOBA) has been studied extensively in recent years, due not only to its monomer being the major component in most of the commercial thermotropic liquid crystal (LC) co-polyesters† but also to the homo-polymer being, in a sense, the generic 'polyethylene' of liquid crystal polymers, in terms of its chemical simplicity and representative transition behaviour. There is a transition to a mesomorphic state[1], most frequently described as the smectic E state[2], at about 340°C for solution polymerized PpOBA, followed by a transition to a lower ordered mesomorphic state at *ca* 445°C[3]. Using a combination of X-ray and electron diffraction (ED), Lieser[4] first identified the coexistence of two orthorhombic phases, I and II, at room temperature, as well as describing the high temperature (above 340°C) phase as being orthorhombic (pseudo-hexagonal) phase III. Phase II was proposed to be most prevalent in low molecular weight material, the relative amount of phase I increasing with polymerization time and temperature. Based on a similarity of the unit cell parameters of phase I with those of poly(*p*-benzamide)[5], he suggested the space group $P2_12_12_1$, with *cis*-conformation, anti-parallel chains, for the structure of PpOBA phase I. In this space group the planes of consecutive phenyl rings along a chain are parallel, but at an angle to those in neighbouring chains. The same space group was also proposed by Geiss and coworkers[6,7] at about the same time, correcting an earlier proposal of a hexagonal crystal structure involving pairs of co-twisted helical molecules[1]. Although Lieser described unit cell parameters for the orthorhombic phase II ($a = 3.77$, $b = 11.06$ Å, with $c = 12.89$ Å for oligomers and 12.6 Å for polymer), the space group was not defined.

In a study by fibre X-ray diffraction of co-polymers of pOBA and 2,6-oxynaphthoate (ONA), Biswas and Blackwell[8] suggested the successive phenyl rings along the chain in homo-polymer PpOBA phase I are rotated by *ca* 120° with respect to each other, in analogy with the conformation proposed previously for poly(*p*-phenylene terephthalamide) (PPTA)[9–11]. In a paper directed primarily at the high temperature phases a similar conformation was proposed by Coulter *et al.*[12] as one of two low energy conformations of PpOBA based on simulating the observed X-ray patterns using molecular models derived from knowledge of preferred intra- and intermolecular conformations of the component moieties (ref. 13, the modelling being based on a forerunner of the

* To whom correspondence should be addressed
† For instance Vectra A950, marketed by Hoechst–Celanese, is the 73/27 copolymer of *p*-oxybenzoate and 2,6-oxynaphthoate

current Cerius[2] program used here, Molecular Simulations, Inc., San Diego, CA). The second form is one in which the phenyl rings (and ester groups) are at a 60° angle. The phenyl rings in both were proposed to have a 'face to edge' interchain packing (see *Figure 3*, below) with the ester groups being nearly planar with the phenyl rings and having, to a degree, carbonyl carbon to carbonyl oxygen contact. The 120° *cis*-conformation is similar to that proposed for poly(*p*-phenylene terephthalate) in the same paper. X-ray patterns obtained from commercial (Ekonol, Carborundum Co.) samples showed an 002 reflection (see below), leading the authors to suggest the presence of domains of parallel and random packing; the anti-parallel packing was ruled out. These samples were totally phase I as shown by the absence of the 020(II) peak (see *Figure 16* below).

Coulter *et al.*'s proposal was followed by Sun *et al.*, again based on X-ray fibre patterns of P(pOBA/ONA) copolymers, proposing a $Pbc2_1$ space group[14] for the conformation and intermolecular packing of PpOBA, a symmetry the same as that proposed by Iannelli *et al.*[15] for PONA based on X-ray fibre patterns. As for the cell proposed by Coulter *et al.*, Sun *et al.* propose that the phenyl rings and the ester groups in a given monomer residue are nearly coplanar, consecutive phenyl-ester planes are rotated by 119° along the *c*-axis, and the chains have a *cis*-conformation.

In one of two recent papers on the crystal structure of PpOBA Iannelli and Yoon have suggested[16] space group $Pbc2_1$ symmetry, *cis*-conformation for both phase I and phase II. They used X-ray diffraction patterns for PpOBA powder obtained from Polysciences, Inc., of unstated thermal history. The data for phase II were obtained by subtraction using an as-polymerized sample of low molecular weight, the two phases co-existing in all of their samples to varying degrees. In their models for both phases I and II the successive phenyl rings are at a 119° angle with the ester unit rotated 9° from the plane of the phenyl ring of its residue, toward the other chain in the same unit cell. They indicated that they got a better fit with the phase I data, particularly for the intensity of the 002 reflection which is not visible in their X-ray pattern, if they assumed a statistical up-and-down arrangement of the chain directions (in agreement with the simulations of Coulter *et al.*[12]), rather than the parallel (all up or all down) packing required by the $Pbc2_1$ space group; this is similar to their conclusions for PONA high temperature solution polymerized material[15].

The other recent paper is a molecular mechanics calculation of the crystal structures by Lukasheva *et al.*[17]. They suggest the most stable form for phase I has an anti-parallel packing of chains with a *cis* conformation and unit cell parameters of $a = 7.47$, $b = 5.16$, $c = 12.64$ Å, c having been fixed at the experimentally observed value, but that other forms of packing (e.g. a *trans*-conformation, in which all carbonyl oxygens are on the same side of the chain) are also possible since the packing energy differences are small. They suggest the significantly smaller calculated values of b than those measured (here $a = 7.45$, $b = 5.64$ Å) is due to the formation of phase I by a transformation from phase II during sample preparation and that their values would be obtained if phase I were formed directly. We note, however, that phase I forms directly if PpOBA is cooled from the LC state, and this also is likely to occur in our samples. For phase II they get unit cell parameters much closer to those observed, but suggest a wide range of unit cells are possible, involving face-to-face and face-to edge, *cis*- and *trans*-conformations, and parallel and anti-parallel packing of the molecules.

Unfortunately, they do not show predicted X-ray powder or ED single crystal diffraction patterns for their different forms, and thus comparison between the published data and the data we present here is not possible without determination of atomic positions for their models. Clearly, however, the different proposed cells for phase II, as we have shown for related models minimized using Cerius[2], would yield significantly different ED patterns, even for [001], and all published single crystal patterns are essentially identical. Furthermore, the number of orders of reflections for both phases (see below) are incompatible with their suggestion of polymorphism at the molecular level in the PpOBA crystals. On the other hand, as considered further in the discussion section below, crystals formed by cooling from the LC state, depending on the thermal and shear history, may well involve various types of defects in the molecular packing similar to those proposed in the papers by Iannelli and Yoon[16] and Lukasheva *et al.*[17].

In the past few years considerable research on the morphology, crystal structure and transition behaviour of PpOBA has been done in our laboratory[18–24]. Our confined thin film melt polymerization (CTFMP) technique[22] permits us to grow lamellar single crystals of both phase I and II PpOBA showing high orders of [001] zone (*hk*0) reflections by ED. By solution polymerization, at high temperatures and low concentrations, we have described the growth of both single crystal whiskers[18] and whisker–disc aggregates[24], again of both phase I and II, with suitable lateral dimensions for ED observation at standard accelerating voltages. With the molecular axes parallel to the whisker axis, these diffraction patterns yield information on various zones containing the molecular axis, e.g. [100], [110] and [010], thus overcoming the cone of diffraction limitation imposed if tilting of lamellar single crystals only can be used. The patterns thus provide much more detailed structure data than is possible from any fibre or powder X-ray diffraction investigations in which significant overlap of reflections will occur, particularly for larger scattering angles.

The ED intensities may, however, be compromised by beam damage, dynamic and secondary scattering and the method of intensity measurement. The former is greatly limited in the case of PpOBA, dynamic scattering can be reduced, effectively eliminated, for light atom crystals (e.g. most polymers) by using high accelerating voltage and thin crystals, and secondary scattering can be reduced by the use of single layer crystals of the CTFMP samples and individual whiskers. Although high voltage was not used, the thinness of the coherent, individual lamellae, 100 Å or less, and half that if bilayered[19], suggests dynamic diffraction would be limited; in paraffin crystals *ca* 60 Å thick dynamic diffraction caused an increase in 220/120 and 310/120 intensities of less than 1.5 for 100 kV electrons[25]. On the other hand, the [001] crystals used often consisted of several essentially incoherent, superposed lamellae, in order to obtain reasonable intensity, and thus secondary scattering is likely. The method of intensity measurement, which seems satisfactory but is a region susceptible to some improvement, is described below.

Utilizing ED data from those studies, complemented by molecular and crystal packing modelling using Cerius[2] and direct phasing techniques[25], we describe here the crystal structures of phases I and II for as-polymerized PpOBA, suggesting the observed crystal structure can be considered as the 'perfect' or 'ideal' structure, with disorder introduced during processing or thermal treatment possibly resulting in some of the previously reported structures. The results are also compared with both published and our own X-ray diffraction scans of powder type samples.

EXPERIMENTAL

Data collection

Details of the process for growing both the solution polymerized and CTFMP samples have been previously described[18,22]. The diffraction patterns chosen for intensity measurements and presentation in the figures are representative of numerous others, being chosen on the basis of the symmetry (lack of sample tilt), non-overlap of several crystals and number of orders seen, taking consideration of the potential for secondary scattering from multi-layer crystals. The solution grown whiskers were dispersed on C-coated grids, the CTFMP samples removed from the glass slides on which grown by floating on HF of various dilutions, samples were coated with Au for *in situ* spacing calibration when desired and observed using various transmission electron microscopes at 100 or 120 kV. Although low beam conditions were used, the samples are considerably more radiation resistant than most polymers.

For determination of unit cell parameters and comparison with the Cerius[2] modelling results, the ED patterns were scanned with a Relisys 9624 scanner and Adobe Photoshop/Art Scan software (grey scale, photo grade, $\gamma = 1$) at a resolution of 1500 dpi for accuracy; the spacings were measured with NIH Image software. A least squares refinement program was used for determination of the cell parameters (Courtesy of A.-Q. Zhang, University of Akron). The scanned patterns, without background subtraction, were also used for the measurement of 'integrated' intensities of the reflections. The spot intensities were converted into peaks by the NIH software using a narrow slit whose width covered the darkest spot among all of the reflections for the pattern used. The peak areas above background were approximated by a triangle, the apices being determined by eye and measured with the software[25]. Observed structure factors (F_0) were calculated assuming a single crystal rather than a mosaic crystal, i.e. $F_0 = kI_0^{1/2}$ where k is a proportionality factor varying from film to film (for a mosaic crystal $F_0 = k(I_0/d)^{1.2}$ where d is the spacing of the reflection)[25]. These values of F_0 were then 'adjusted' by a constant factor for comparison with the Cerius[2] predictions by minimizing the differences between the F_0 and the F_c.

X-ray diffraction scans were taken using a Rigaku Denki Geiger Flex D-Max IIIa diffractometer in reflection mode, with Ni-filtered Cu–K_α radiation. Filtered, powder type samples of bulk solution (Therminol 66 or Marlotherm S*) polymerized PpOBA of disc and whisker morphology were examined, polymerization conditions are described in the text below.

Modelling using Cerius[2]

The crystal structures of PpOBA phases I and II and its chain conformation in the lattices were modelled using the Cerius[2] (1.6) software with the Dreiding force field for an infinitely periodic system. The intramolecular interactions utilized (valence terms) include bond stretching, angle bending, torsional and inversion terms. The intermolecular interactions include van der Waals and Coulombic terms. For our periodic system the Ewald summation method was used in the minimizing calculations. Van der Waals interactions between atoms separated by three bonds are excluded from the energy term. Other parameters were usually chosen as the default options except in those cases in which settings were recommended in the manual for polymer-type periodic systems. A minimized chemical repeat unit of a single molecule was used to build the unit cell. As discussed below, the ester bond torsion factor was varied in the minimization process to obtain the best fit with the [001] pattern; the default value is 0.4. Relative rigid shifting (translation and rotation) of the molecules following minimization was done, as suggested, to improve the agreement with the whisker patterns, comparison with the patterns being done after each small shift. For the simulated electron and X-ray diffraction patterns a global isotropic temperature factor of $6B_{iso}$ (Å^2) was used for phase I, and 7 Å^2 for phase II. With a smaller B resulting in an increase of F_c with increasing angle, the effect of decreasing B on F_c is the same as the effect of assuming a mosaic rather than single crystal for the calculation of F_c. A crystal thickness of 50 Å was used for the ED pattern displays. Contrary to a recent publication[26], varying the crystal thickness only changes the simulated length of the reciprocal lattice rods as they intersect the sphere of reflection and does not incorporate corrections for double diffraction; a smaller crystal thickness results in higher order reflections being shown in the simulated pattern for a given zone. The values of F_c are independent of the crystal thickness chosen. For the X-ray diffraction pattern simulations a crystal size of 500 Å was used.

Direct phasing

Although the space groups ($Pbc2_1$ for phase I, $Pca2_1$ for phase II) are non-centrosymmetric, the plane groups pgm and pmg, corresponding to the [001] projections of phases I and II are centrosymmetric. On the other hand, the [010] projection of phase I, with parallel packing, is non-centrosymmetric, whereas the anti-parallel packing would be centrosymmetric. The following direct phasing method was used to determine the correct structures, as described in detail in ref. 25. A Wilson plot was carried out with observed intensities using $\ln\langle I_{obs}/\sum f'^2_i\rangle$ vs $\sin^2\theta/\lambda^2$, yielding overall temperature factors $B_{iso} = 6.1$ Å^2 for phase I and $B_{iso} = 7.0$ Å^2 for phase II, where f'_i are the atomic scattering factors, for the [001] patterns; the [010] phase I pattern, on the other hand, gave a B_{iso} value near 0.0 Å^2. The latter value is an often observed indicator of a contribution from multiple scattering (dynamic and secondary)[27,28]. Next, the observed intensities were converted to normalized structure factors by $|E_h|^2 = I_{obs}/\varepsilon\sum f'^2_i$, where $\varepsilon = 2$, compensates classes of

* Trademarks of Monsanto Co. and Huls America, Inc. for heat transfer fluids

reflections with systematic absences. The values of $|E_h|$ were used to rank the phase invariant sums (so-called $\sum_2$-triples) in order of decreasing probability according to the values of $A = (2/N^{1/2})|E_h E_k E_{h-k}|$. After generating this set of simultaneous equations for the phases, an origin is defined by arbitrarily assigning the phase values to two zonal reflections with index parity $h_i k_i l_i \neq$ eee or where $\sum h_i k_i l_i \neq$ eee.

For the [001] projections, the origin was defined by assigning phases of two strong reflections $\phi_{110} = \phi_{250} = 0$ for phase I, $\phi_{110} = \phi_{320} = 0$ for phase II. A third strong reflection was given an algebraic term $\phi_{020} = a$ for phase I and $\phi_{10\,00} = a$ for phase II, where a is a variable that represents the unknown phase 0 or π, for the centrosymmetric projections, in order to access enough reflections during solution of the simultaneous equations. With this set of assigned phases as a basis, the phases of other reflections of lower $|E_h|$ value can be determined by phase expansion (symbolic addition) process. The electrostatic potential maps were generated based on the intensity amplitudes and phases. For each form (phases I and II), two maps with $a = 0$ or π were generated and the correct one is usually recognizable. Fourier refinement could not be carried out for the [001] projections because atomic positions could not be identified due to eclipsing of positions in the projection along the polymer chain. For the Phase I maps shown here $F(000)$ was assigned a value of 0.0, resulting in positive and negative contours, whereas for Phase II the sum of the scattering factors in the unit cell at $\sin\theta/\lambda$ was set equal to 0.0; the result is a difference in scaling but no change in the positions of the density profiles in the structure.

The whisker phases were determined (in plane group pg, assuming a 2_1 screw axis along c) by using the Sayre equation after defining two origin phases and accepting two more values from high-probability $\sum_1$-triple invariants. One algebraic phase term was permuted ±45°, ±135° to generate four potential maps after phase extension. After identifying a likely solution in one of the maps, the possible atomic positions were used to calculate structure factors and this began the Fourier refinement process (see *Figure 11*) to find the remaining atomic positions, all of which appeared in successive maps in a reasonable representation of the projected structure.

RESULTS

Phase I

Morphological observations of PpOBA lamellar, disc and whisker single crystals polymerized at several temperatures in various solvents[20,24] and lamellar single crystals and single disclination domains prepared by the CTFMP technique[19,22] have been described in detail. A diffraction pattern from a non-Pt-shadowed, non-Au-decorated CTFMP crystal (*Figure 1*, polymerized for 3 h at 180°C) was used for the [001] intensity data used below to prevent possible double diffraction involving the Au or Pt. The intensity distribution, however, is similar to that in shadowed and/or decorated samples of other melt polymerized (CTFMP[19,22] and bulk[23]) PpOBA lamellae. With {260} being visible on the negative for *Figure 1*, intensities could be measured for 39 independent reflections; all of the measured intensities are listed in *Table 1* in terms of $|F_0|$.

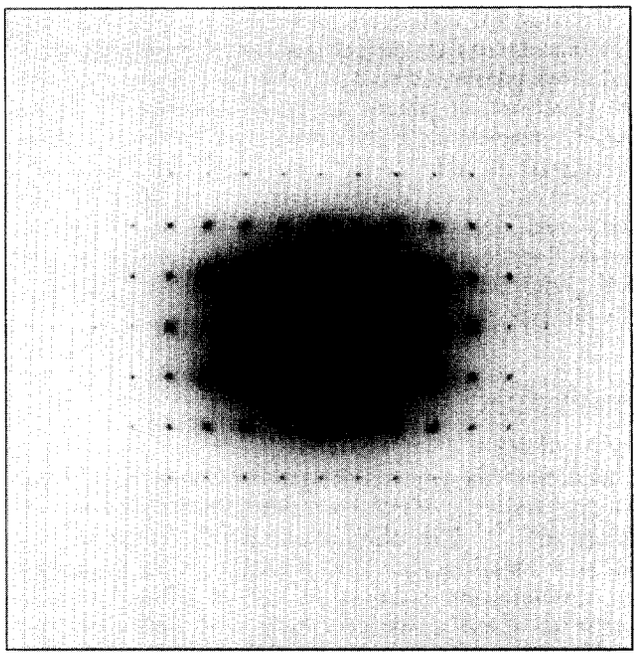

Figure 1 Phase I ED patterns from a CTFMP crystal polymerized for 3 h at 180°C (no Au coating or Pt shadowing)

Table 1 Structure factors of Pp0BA phase I crystals

hkl	$\|F_0\|$	'I&Y' $\|F_c\|$	Our $\|F_c\|$	*hkl*	$\|F_0\|$	'I&Y' $\|F_c\|$	Our $\|F_c\|$
100	4.04	3.80	4.00	030	3.25	0.01	0.02
200	42.10	41.53	43.76	130	4.06	0.72	1.08
300	5.34	0.53	3.23	230	4.74	1.98	3.63
400	9.87	1.11	2.05	330	2.99	0.14	0.71
500	2.90	2.01	0.73	430	3.31	0.15	1.18
600	3.27	1.33	1.53	530	1.46	0.14	0.61
010	4.42	0.02	0.04	630	0.64	0.67	0.64
110	30.91	32.05	30.89	040	1.66	0.08	1.68
210	12.58	11.82	12.57	140	1.63	1.99	1.65
310	15.73	13.33	14.36	240	1.82	1.22	1.87
410	7.05	5.72	5.66	340	2.09	2.03	2.45
510	6.26	1.84	3.21	440	0.51	1.07	1.30
610	0.97	0.83	0.58	640	0.49	0.04	0.35
020	9.11	4.05	3.79	150	2.37	2.66	3.80
120	8.08	7.51	6.61	250	0.28	0.11	0.28
220	8.71	3.49	2.35	350	0.44	0.80	1.21
320	8.75	8.55	9.13	450	0.25	0.08	0.08
420	6.48	4.99	5.25	060	1.37	1.62	1.67
520	4.04	2.62	3.20	260	0.41	0.78	1.01
620	1.56	0.78	1.96				

R-Factors; 'Iannelli & Yoon', 0.303; Our, 0.263

Figures 2a, 2b and *2c* show typical solution grown whiskers of PpOBA and resulting phase I [100] and [110] ED patterns. Direct observation, the patterns corresponding to the appropriate planes of the reciprocal lattice, shows that the crystals are metrically orthorhombic ($\alpha = \beta = \gamma = 90°$). Using [001] pattern from both solution and melt polymerized crystals and the whiskers, all with *in situ* Au for spacing calibration, and a least squares refinement (program courtesy of A.-Q. Zhang, University of Akron), the unit cell dimensions are a = 7.45, b = 5.64 and c = 12.47 Å, with a calculated density (two chains per cell) of 1.523 g cm^{-3}. These values are close to those reported by Iannelli and Yoon (a = 7.42 Å, b = 5.70, c = 12.45 Å, p = 1.515 g cm^{-3})[15], but significantly larger than the lattice parameters proposed by Lukasheva *et al.*[17] for their phase I structures.

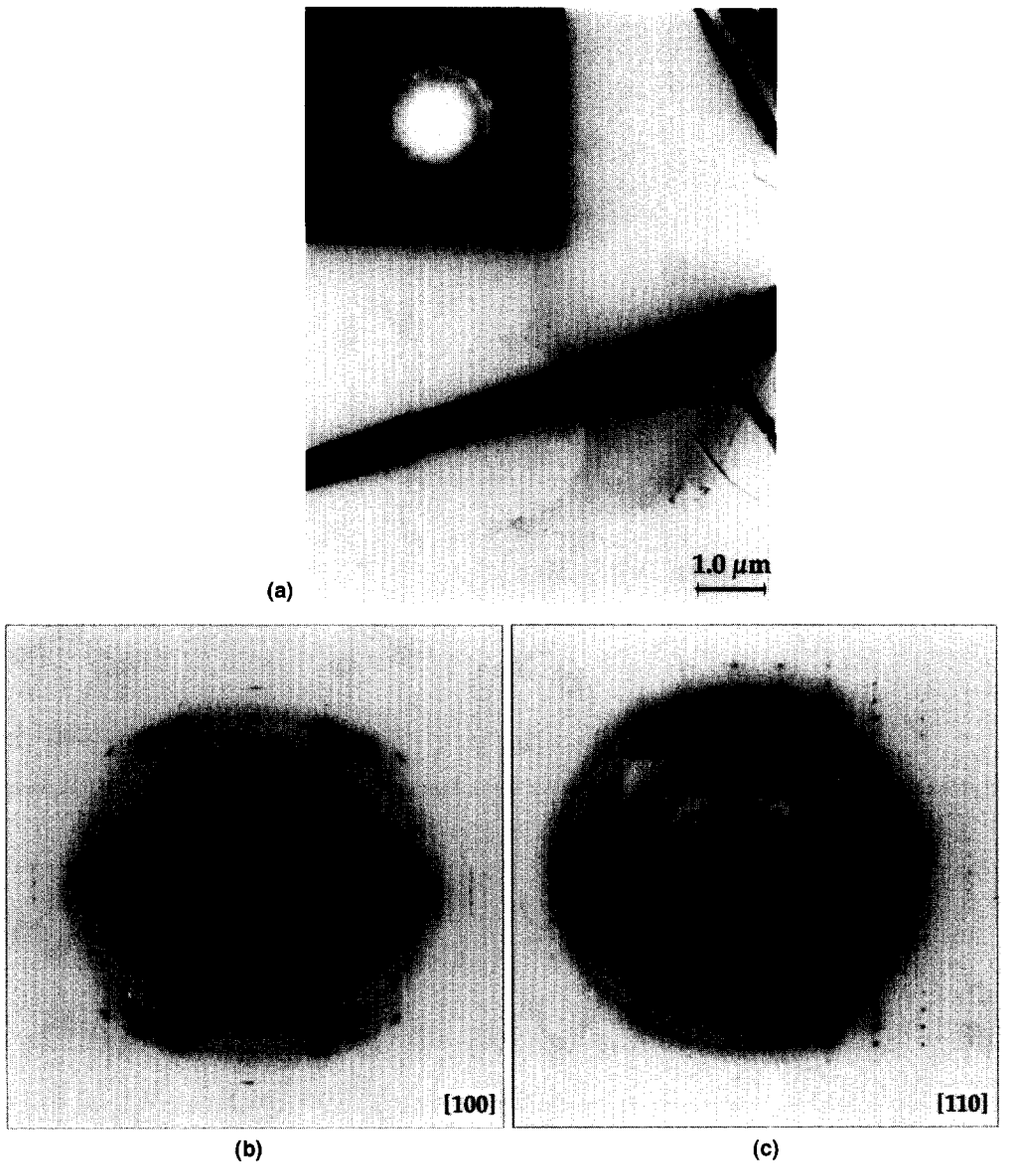

Figure 2 (a) Single crystal whiskers of PpOBA polymerized in a 1% solution of ABA in Therminol 66, at 350°C for 21 h. The inset ED pattern is from the area in the circle and is properly oriented (b) and (c) phase I [100] and [110] ED patterns from similar whiskers

The very strong {200} and {110} reflections in the [001] pattern (*Figure 1*) are common features in the ED [001] patterns for most two chain unit cell, lamellar, crystalline polymers, whether prepared by CTFMP as extended chain crystals or by chain folding of already polymerized polymer from solution or the melt. It suggests that one of the two chains is at x_1, y_1 and the other at $x_2 = 1 - x_1$, $y_2 = 1 - y_1$ where x_i, y_i are the coordinates of equivalent atoms in chains 1 and 2 in the [001] projection. Another feature of the [001] pattern shown is the relatively strong intensity of the {150} and {060} reflections at their high order positions; this cannot be primarily due to dynamic diffraction or secondary scattering, the nearby reflections of lower order being considerably weaker. The absence of significant multiple scattering in this pattern is also shown by the value of B_{iso}, which is in accord with typical values for organic samples[25]. The large number of [001] reflections is attributed to the high crystallinity, thinness of the crystals and/or some degree of (symmetrical) bending, the decrease in intensity in all patterns at the higher angles (060 and 0.0.12 have spacings of <1 Å) to the first minimum of the atomic scattering factors.

In the [100] pattern in *Figure 2b* the intensity of all of the *ca* 150 reflections are also symmetrically distributed. This was less frequently the case than for the lamellae; the whiskers in many of the preparations have a more or less circular cross section and thus the reciprocal lattice plane can easily lie at an angle to the substrate. Although relatively rigid, kinks forming if bent sharply[24], gradual curvature did contribute to arcing of the reflections in some cases. Among the reflections shown {002}, {006}, {023}, {029}, {033}, {039} and {048} are considerably stronger than their neighbouring reflections. A significant feature of the [100] pattern is that the $0k\ell$ row lines have reflections for all values of k; the reflections with k odd are forbidden for the $Pbc2_1$ space group proposed by Iannelli and Yoon[16]. The presence of the k odd reflections, with the 03ℓ row being particularly strong, indicates that the two molecules are either staggered along the c-axis (see below) or shifted along the b-axis from the b glide symmetry positions. The absence of 00ℓ reflections with ℓ odd suggests at least a pseudo 2_1 screw axis symmetry, indicating the c-axis staggering, if present, must be small. The absence of 00ℓ reflections with ℓ odd also suggests a minimal contribution from secondary scattering in the whisker patterns. Dynamic scattering

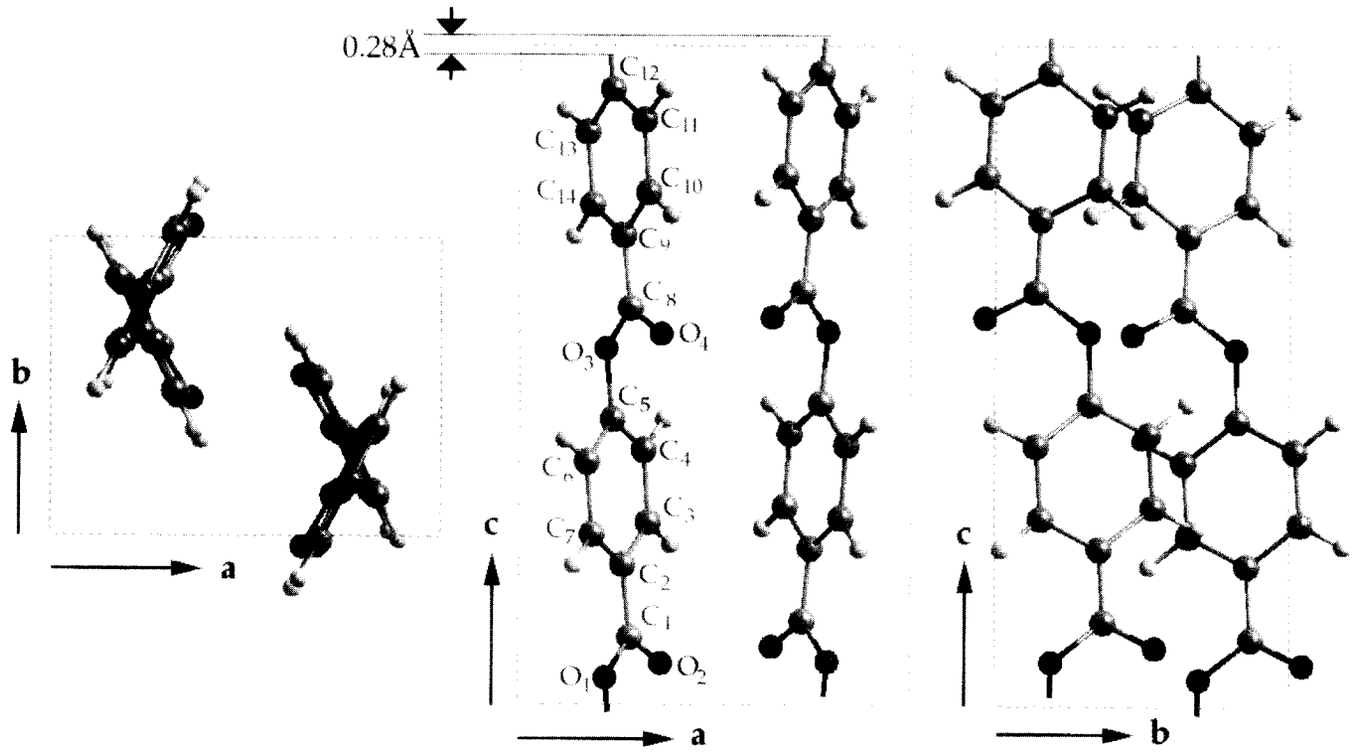

Figure 3 Proposed phase I PpOBA unit cell based on the patterns shown in *Figures 1* and *2*. Packing energy is $-177.9\,\text{kcal mol}^{-1}$

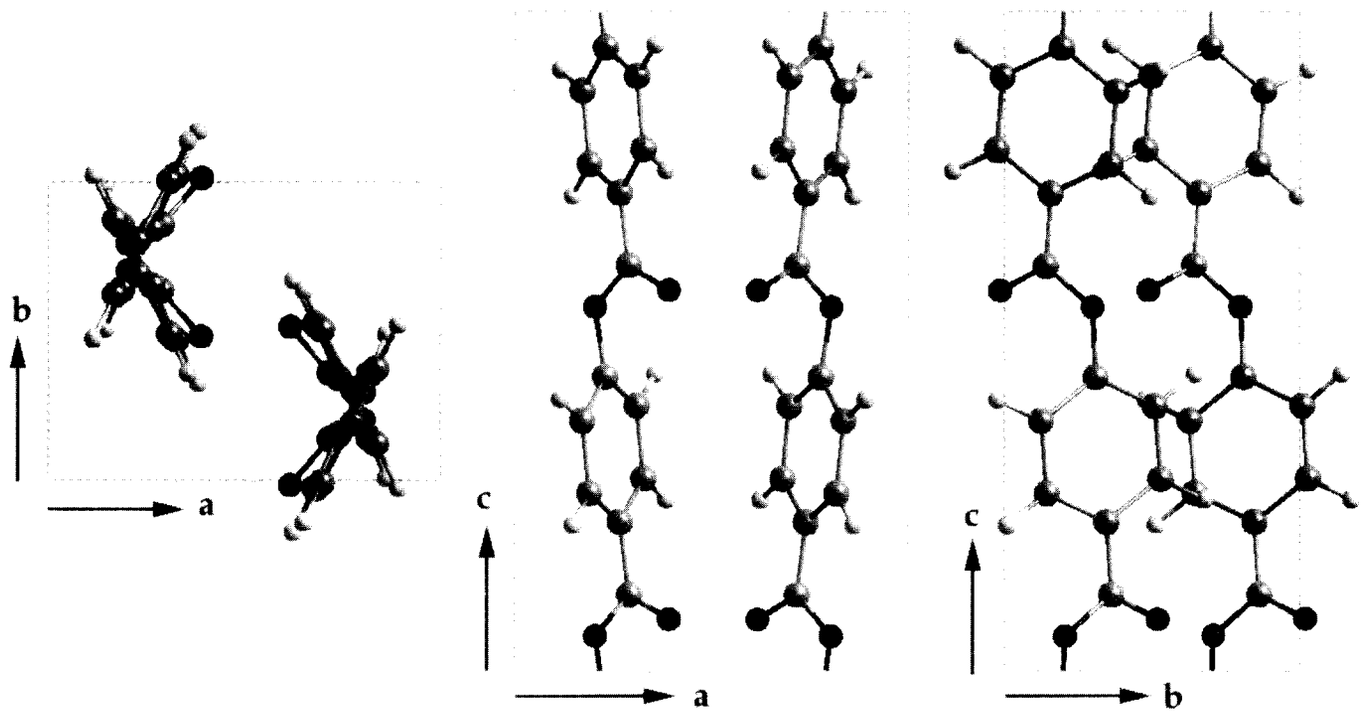

Figure 4 'Iannelli and Yoon' cell as modeled by Cerius[2] for the $Pbc2_1$ parallel packing and our unit cell parameters. Packing energy is $-182.6\,\text{kcal mol}^{-1}$

could still be playing a role, however, as indicated by the value of B_{iso}. As shown by the simulated ED pattern in *Figure 5c* below, a small *c*-axis stagger gives good agreement with the observed pattern; the *b*-axis stagger, however, although yielding $0k\ell$ row lines with k odd, gave an incorrect intensity distribution on those row lines for all small staggers tested. Furthermore, neighbouring pairs of identical conformation molecules, with one common molecule, would have different separations for the molecules within the pairs, there is no reason this should occur.

In the [110] pattern in *Figure 2c* the distribution of intensities is asymmetric, those on the right being more intense than those on the left, but nearly symmetric on the $\pm\ell$ sides, suggesting a rotation of the lattice about the whisker axis. In this pattern {002}, {006}, {110}, {111}, {113}, {223}, {119} and {229} are clearly stronger than their neighbours, despite the asymmetry of the pattern.

The result of simulating the chain conformation and molecular packing of PpOBA using the Cerius[2] program that is in best agreement with the ED patterns is shown

in *Figure 3*. In agreement with the suggestions of Sun *et al.*[14] and Iannelli and Yoon[16], the ester groups in the [001] projection are essentially parallel to the phenyl rings, ours lying even closer to parallel than those of Iannelli and Yoon. Successive phenyl rings lie at an angle of 124°. However, the chains in the [100] projection are staggered, by 0.14 Å each, in opposite directions from their positions defined by the screw symmetry in the $Pbc2_1$ space group cell shown in *Figure 4* and are parallel. The latter would be in agreement with our morphological observations which suggest parallel, but opposite direction growth from a midline, for polymerization–crystallization in solution[20]. A table of the fractional atomic coordinates, from which interatomic distances and angles can be calculated, is given in *Table 2*. The 'Iannelli and Yoon' model in *Figure 4* was simulated starting with the conformation and packing proposed by Iannelli and Yoon for the parallel packing model and using a torsion factor of 0.0 for the ester bond. For the cell in *Figure 3* a torsion factor of 0.2 was used; a value of ≥ 0.3 yields an [001] projection in which the ester groups lie on the 100 plane, i.e. lie on a plane bisecting the near 60° angle between successive phenyl rings. For all three cells, before introducing the stagger, the [100] projection is nearly indistinguishable. Although the packing energy for the staggered model is slightly higher than that for the Iannelli and Yoon model (−178 vs −183 kcal mol^{-1}), this is attributed to the torsion factor. Before staggering the model in *Figure 3* had a packing energy of −164 kcal mol^{-1}; i.e. staggering reduces the packing energy.

Figure 5 shows the calculated [001] ED patterns based on the simulations in *Figures 3* and *4* and for the 'bisection' model. Stagger along *c* does not affect this projection since the chains were shifted rigidly along *c* after minimization. A comparison of the simulations with the pattern in *Figure 1* and those from the CTFMP[22] and solution polymerized[17] samples suggests better agreement for the model in *Figure 3*, particularly for the higher order reflections which are most influenced by the details of the atomic arrangement. However, both the Iannelli and Yoon model and the bisection model also show reasonable agreement in terms of visual observation only and none of the patterns show perfect agreement. For instance, for all of the models 010 and 030 should be very weak whereas 010 is slightly more intense than 100, a feature that cannot be due to strong secondary scattering from any of the strong, neighbouring reflections. It could, however, arise from $\bar{2}00$ and $\bar{1}10$ reflections for which the 210 and 120 reflections are the incident beams. The intensity of 400, 220 and 330 also all appear too strong relative to the ED simulations in *Figures 5a* and *5b*; although the enhanced intensity of 400 and 220 can be due to secondary scattering from the 110 and 200 reflections, 310 should be enhanced by the same secondary scattering but has the predicted intensity, and 330 should not result from secondary scattering. It is noted direct visual comparison can be somewhat misleading. For example, the intensity for 100 in the simulations in *Figures 5a* and *5b* appears much too strong relative to 200 but the data in *Table 1* show good agreement. These patterns have been printed with a large 'incident intensity' to display the higher order reflections; as a result the strongest reflections appear to saturate, making visual comparison difficult.

The better agreement for the model in *Figure 3* is confirmed by comparison of observed and calculated structure factors listed in *Table 1*. The F_c values listed for the Iannelli and Yoon model are those from the Cerius[2] program multiplied by a constant factor corresponding to the ratio of the adjusted F_0 for the 200 reflections for the two models; minimization of the differences in F_c and F_0 for the two models results, initially, in different F_0(Adj.) for the two models. The resultant *R*-factor (for [001]) only) is 0.26 for our cell and 0.30 for that of Iannelli and Yoon; the *R*-factor was not calculated for the bisection model. Both values are somewhat larger than the values 0.14, 0.22 and 0.23 we have obtained for

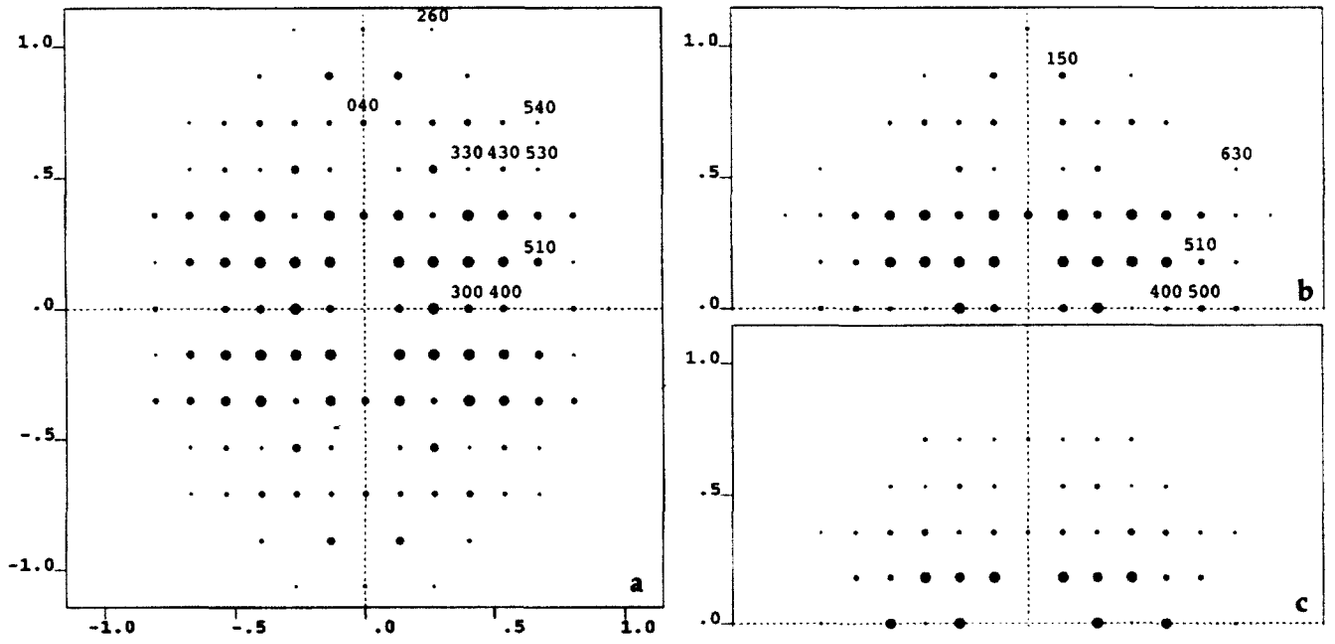

Figure 5 (a) and (b) Simulated [001] ED patterns for the phase I cells shown in *Figures 3* and *4*, respectively. The pattern in (c) corresponds to the bisecting model in which the ester groups lie on a plane parallel to *a*. In this and some of the following figures only a portion of the simulated ED pattern is shown; in all such cases the pattern is symmetrical

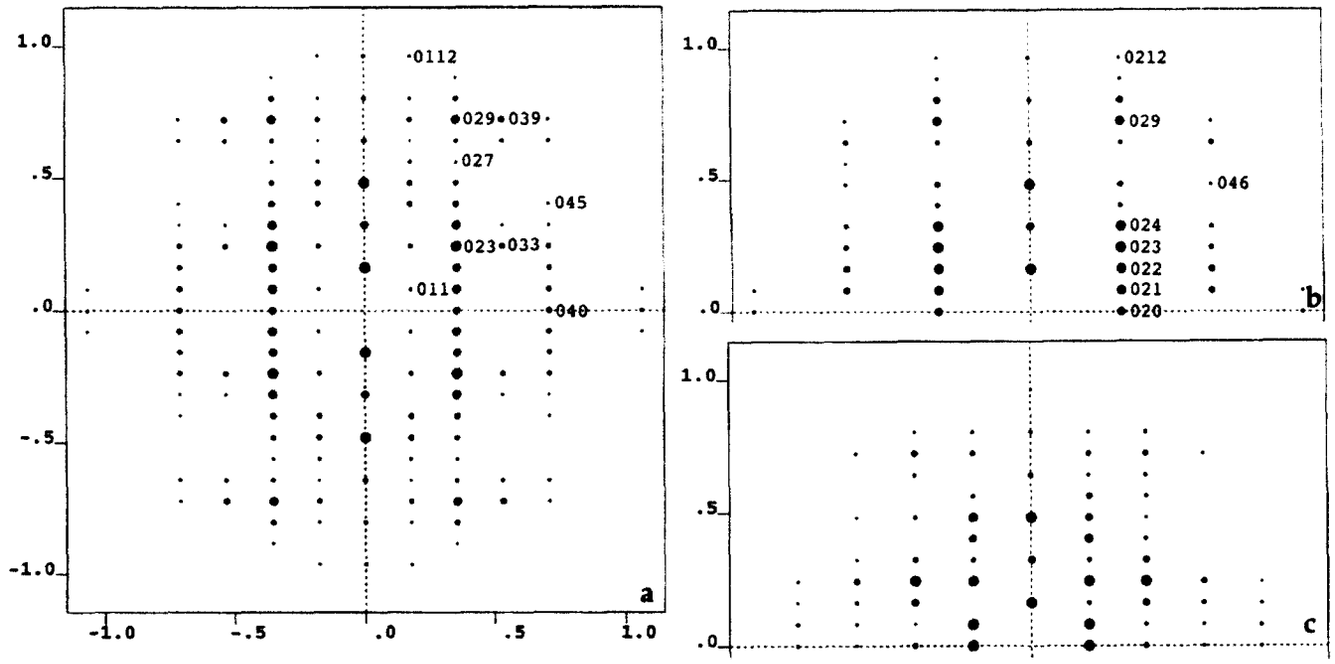

Figure 6 (a) and (b) Simulated [100] ED patterns for the staggered and $Pbc2_1$ cell. (c) Simulated [110] ED pattern for the staggered cell

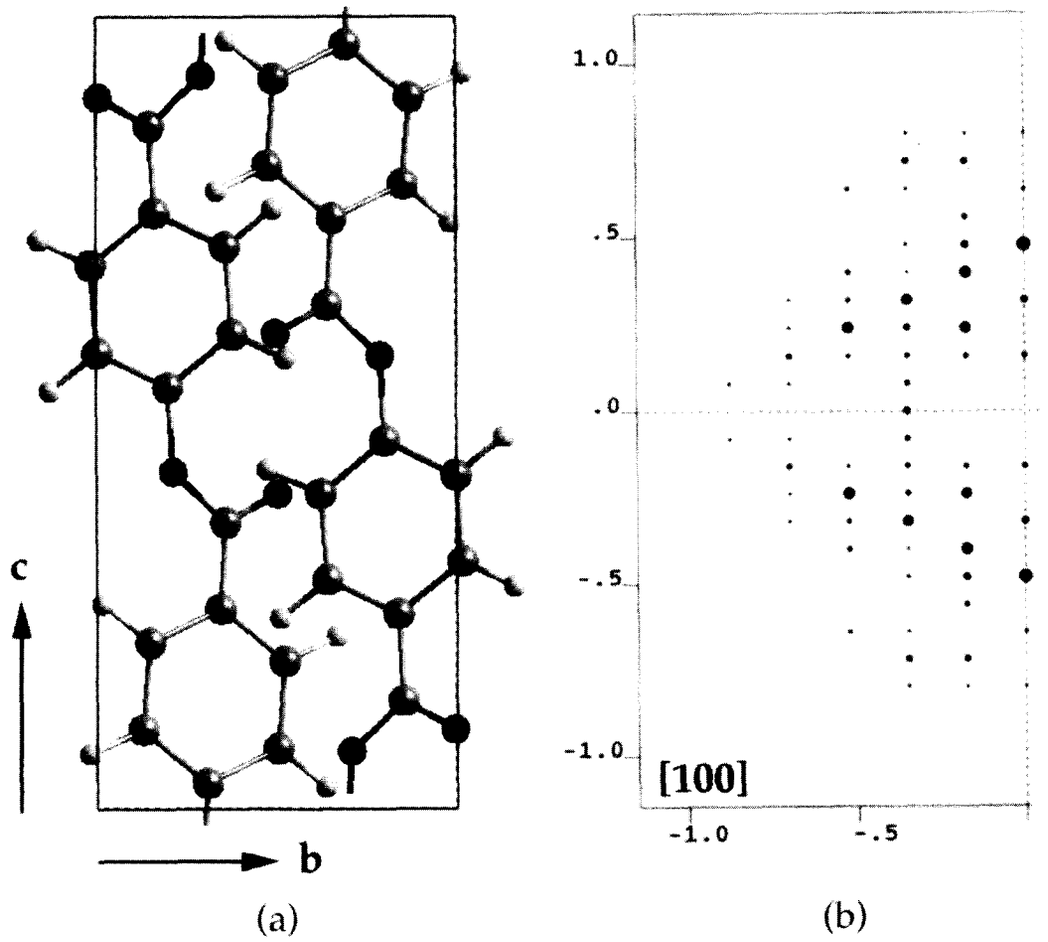

Figure 7 (a) [100] projection and (b) simulated [100] ED pattern for the anti-parallel packing, $P12_1/c1$ cell using our cell parameters. Packing energy is $-168.1\,\text{kcal mol}^{-1}$ for a torsion factor of 0.2

the three dimensional packing of poly(butylene terephthalate)[29], poly(ethylene terephthalate)[30] (PET) and poly(terephthalic anhydride)[31]; the larger value is attributed to residual multiple scattering even though B_{iso} is 6.1 (Å^2).

As shown by the patterns in *Figures 6a* and *6b*, the simulated staggered cell [100] pattern is clearly much closer to that observed than is the pattern from the $Pbc2_1$ cell. The [100] pattern for the bisection cell without stagger also does not have $0k\ell$, k odd row lines, but if

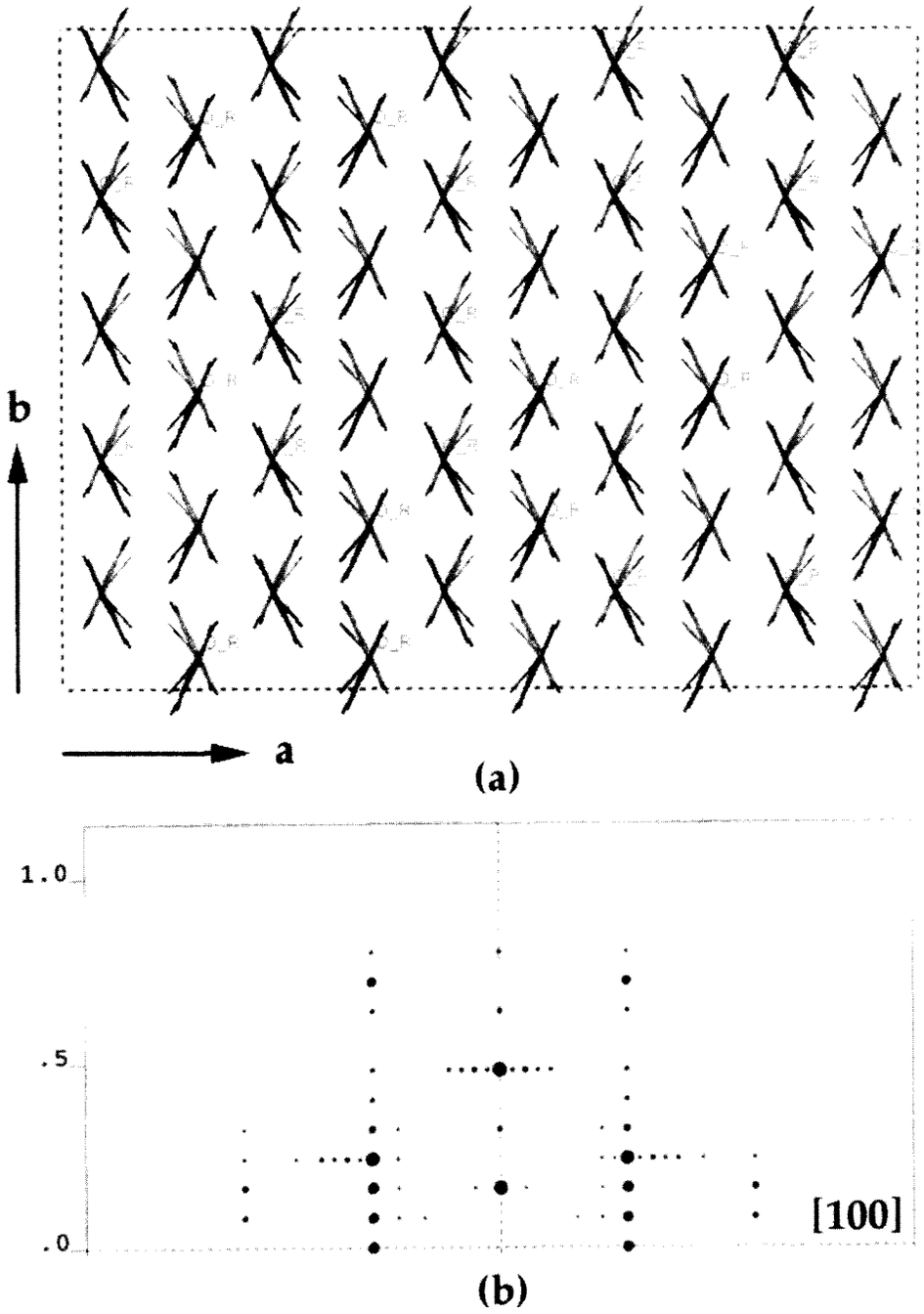

Figure 8 (a) [001] projection and (b) simulated [100] ED pattern for a 5 × 5 unit cell superlattice in which 1/2 of the molecules (those for which the ester groups are indicated by letters) were inverted before minimization

staggered by an equivalent amount 'gives' an essentially identical pattern to that in *Figure 6a* (the major difference is on the 06ℓ row line, 060 and 061 being absent but 062 being present). The [110] pattern for the staggered cell (*Figure 6c*) also has a distribution close to that observed (*Figure 2c*). The diagonally opposite quadrants of this simulated pattern are identical, but neighbouring quadrants have a different distribution of intensity. The asymmetry (compare, e.g. 112 with $\bar{1}12$), despite the apparent symmetry of the unit cell, appears to be a problem with the Cerius[2] program; we have observed it in other cases as well and it is present in the demo supplied with the program for poly(*p*-phenylene terephthalate) which does not have the possibility of a direction to the backbone of the molecules.

Of obvious concern relative to the suggestions of Iannelli and Yoon is whether either an anti-parallel or statistical up-down packing of *cis*-conformation molecules could yield the extra rows of reflections. The [100] projection of the Cerius[2] minimized, torsion factor 0.2, anti-parallel packing (space group $P12_1/c1$), and corresponding ED pattern are shown in *Figure 7*. The [001] projection and simulated ED pattern were the same as in *Figures 3a* and *5a*. Although the 0$k\ell$, k odd row lines are seen, the intensity distribution is clearly incorrect with the 01ℓ having strong 013 and 015 reflections. A simulated random 50/50 up-down packing, based on a 50 chain cell and the resulting [100] pattern is shown in *Figure 8*. In a larger crystal the rows of spots on some of the layer lines would be continuous streaks; these streaks were present only on the [100] pattern, being absent on the [110] and [010] simulated patterns. They were not

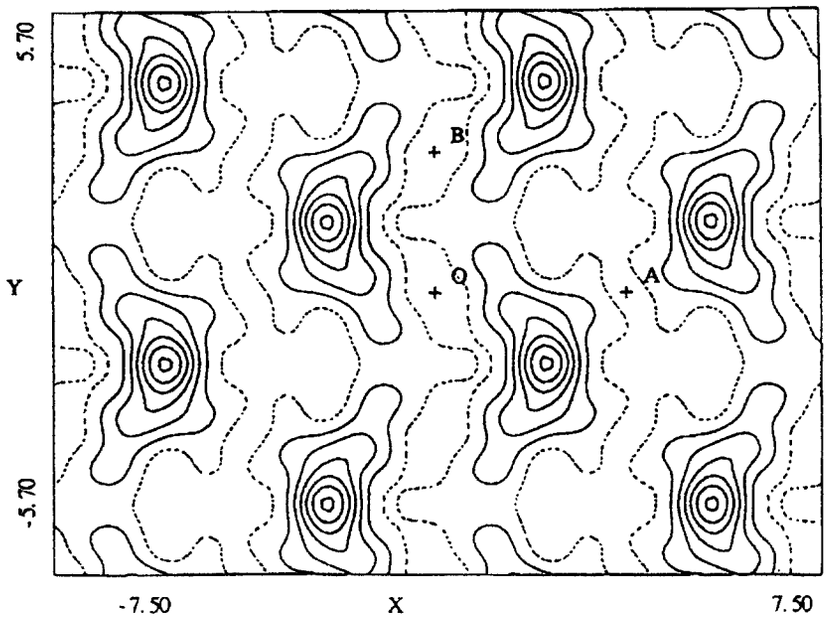

Figure 9 [001] potential map obtained by direct phasing using a CTFMP single crystal phase I ED pattern. For this figure and *Figure 10* F(000) was set equal to 0.0; the dashed contours correspond to 'negative' values of electron density

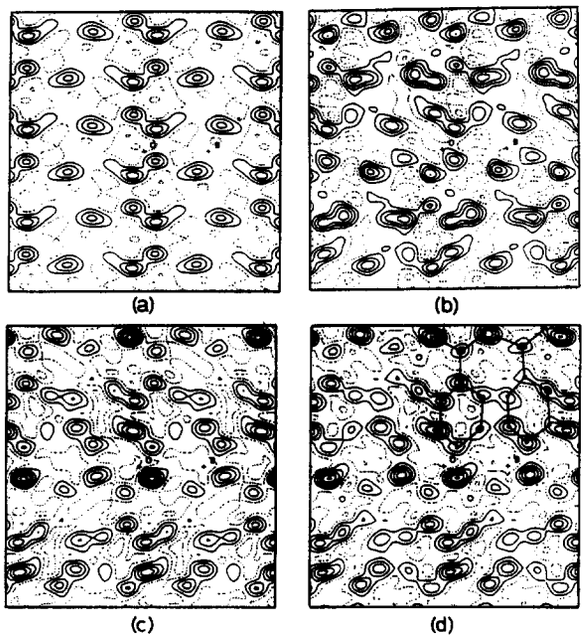

Figure 10 [100] potential maps obtained by direct phasing using a phase I whisker ED pattern. The figures (a–d) correspond to successive stages of refinement

seen on the ED patterns from the whiskers; as shown in *Figure 2*, {002}, {006} and the rest of the reflections were spot-like. $0k\ell$, k odd reflections are not seen in the simulated pattern. It is noted that while the $0k\ell$, k odd reflections might be resolvable in X-ray patterns, such as those of Iannelli and Yoon, the more intense are at large angles and thus overlap with numerous other reflections; furthermore the layer line streaks would not be seen on a powder pattern, other than as a broadening of the appropriate reflections.

For comparison with the suggestions of Lukasheva *et al.* simulations for the four possible 'phase I' cells with a *trans*-conformation and resultant [001] and [100] ED pattern using the same unit cell parameters as for *Figure 3* were made; there are two ways to pack the *trans* molecules in the cell; with the carbonyl oxygens on the two chains in the cell pointing in the same or opposite directions, as well as having the chains in a parallel or anti-parallel direction. The packing in all four possible cells is face-to-edge, the phenyl rings lying at an *ca* 60° angle. None of the ED patterns agree with those observed. If domains of various types of packing, with common axes, existed in the crystals, the resulting patterns would consist of the addition of the appropriate amounts of these patterns and those shown in *Figures 5*, *7* and *8*. While this is possible, we do not believe it occurs in our samples.

The result of initial applications of direct phasing are shown in *Figures 9* and *10*. The [001] potential distribution, using a pattern from a CTFMP crystal lamella, is shown in *Figure 9*. As would be expected, there is a high electrostatic potential along the planes of the phenyl-ester groups, the angle being 120°. However, there is a suggestion the ester group lies at an angle of *ca* 12° to the phenyl rings, i.e. further outside than even proposed in the Iannelli and Yoon model. The calculated [100] potential distribution for four stages of refinement, is shown in *Figure 10*. Superimposed on the final refinement (*Figure 10d*) are outlines of single chemical repeats of the molecules as suggested by the potential maxima. The displacement of the molecules along c can be clearly seen. Although the phenyl rings appear slightly distorted, there is a close match overall with the model in *Figure 3c*. However, the C5–O3–C8 bond lengths and angles differ to a degree from those in *Figure 3c*, the overall phenyl–phenyl ring distance being less and the rings being displaced laterally a small amount in the [010] direction relative to that in *Figure 3*. Although the two modelling methods have used different sets of data, both in terms of the actual negatives and the intensity measurements, this is not believed the cause of the differences. The possibilities of significant multiple scattering perturbations for this projection (indicated by the low temperature factor from the Wilson plot) and the assumption of a 2_1 screw along c for the direct phasing, are being examined at present, as well as the use of the same data

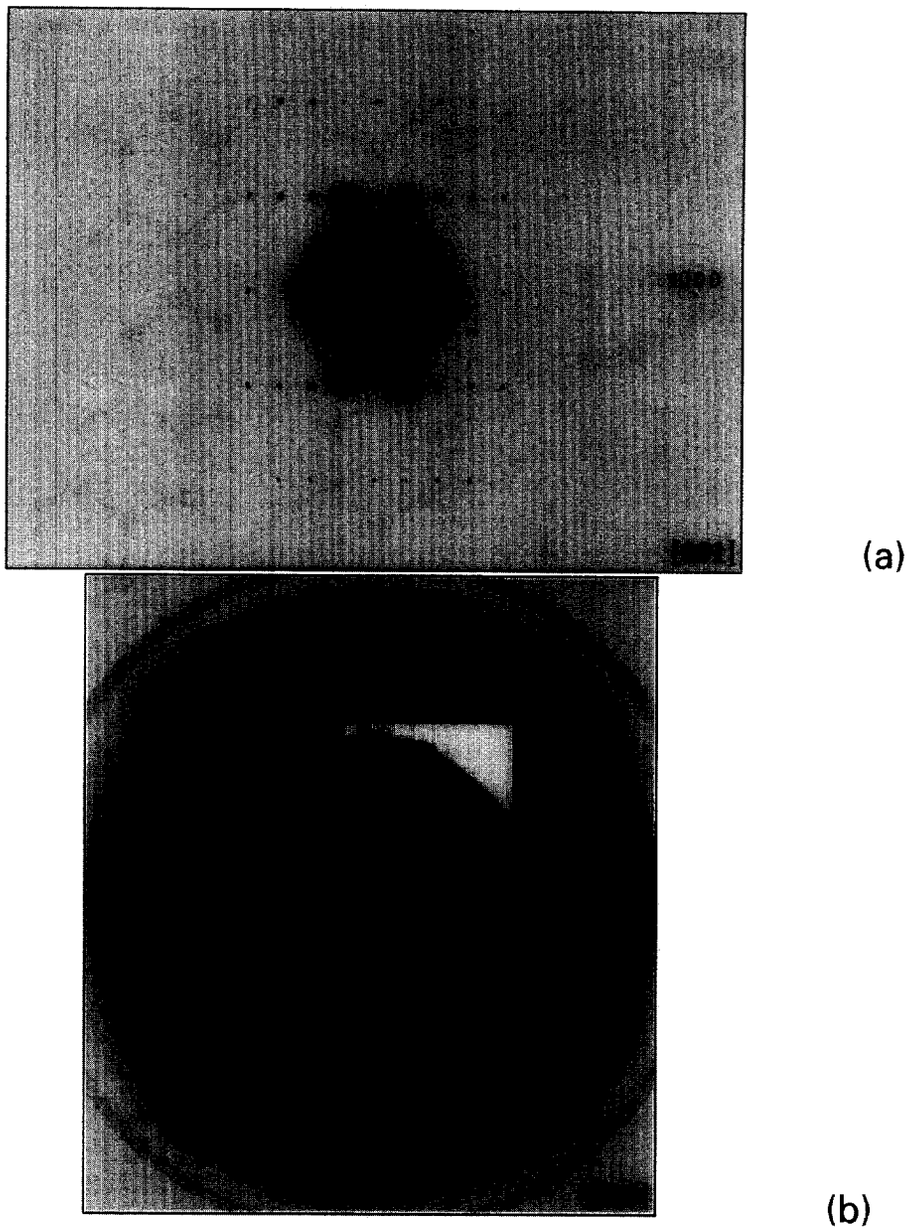

Figure 11 (a) [001] and (b) [010] phase II ED patterns from, respectively, a CTFMP single crystal and a whisker

for both methods. The assumption of the 2_1 screw, in particular, likely leads to the C5–O3–C8 bond distortions, this being the result if a 2_1 screw is imposed on the Cerius[2] model.

Phase II

CTFMP crystals without Pt shadowing or Au decoration were also used for the [001] phase II ED patterns on which intensity measurements were made. Representative micrographs are shown in ref. 22, with an ED [001] pattern from a crystal polymerized 3 h at 180°C in *Figure 11a*. Of particular interest in connection with the calculated pattern below are the relatively strong intensities of {10.0.0}, {020}, {220} and {320}. Phase II whisker patterns (*Figure 11b*) were found only infrequently. This is primarily due to the increase in the relative amount of phase I with polymerization temperature and also, in part, due to the complementarity of the lattice, $a_I \cong 2b_{II}$ and $a_{II} \cong 2b_I$. The latter makes it difficult to distinguish phase I and phase II whisker patterns in the transmission electron microscope solely on the basis of the lateral spacings of the vertical row lines. In the pattern shown in *Figure 11b*, for instance, the first vertical row line (20ℓ) has the same lateral spacing as the 'forbidden' 01ℓ row line in *Figure 2b*. The intensity distribution, although similar, differs to a degree, the reflections on the $2h$ odd row lines being considerably stronger than those on the k odd row lines in the pattern in *Figure 2b*. The unit cell parameters obtained by least squares refinement are $a = 11.15$, $b = 3.80$, $c = 12.56$ Å, with a calculated density of $1.499\,g\,cm^{-3}$. These values are also close to those of Iannelli and Yoon ($a = 11.16$, $b = 3.83$, $c = 12.56$ Å, $\rho = 1.486\,g\,cm^{-3}$)[16]. {006} (and {002} and {029}) are streaked parallel to the layer lines, suggesting translational disorder along the c-axis. The corresponding phase I whisker reflections, as noted above, are spots.

Our proposed unit cell, as modelled by Cerius[2] with a torsion factor of 0.2, is shown in *Figure 12*. Parallel packing, with $Pca2_1$ space group symmetry and a *cis* conformation, is proposed, i.e. the same as proposed by Iannelli and Yoon except for the change in labels of the a and b axes (Iannelli and Yoon[16] follow the description of the axes proposed by Lieser[4] for phase II, with $b > a$).

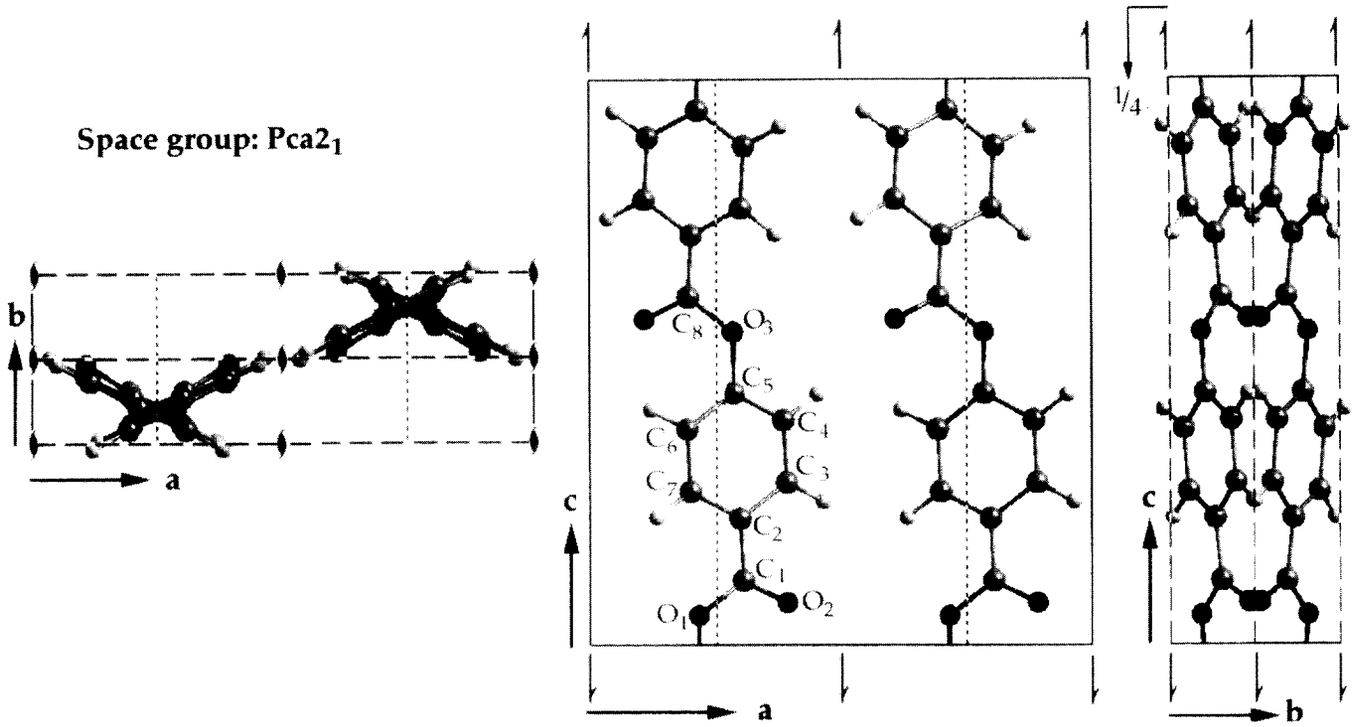

Figure 12 Simulated $Pca2_1$ symmetry, phase II unit cell with parallel, *cis*-conformation molecules based on the patterns shown in *Figure 11*. Packing energy is $-178.1\ \text{kcal mol}^{-1}$

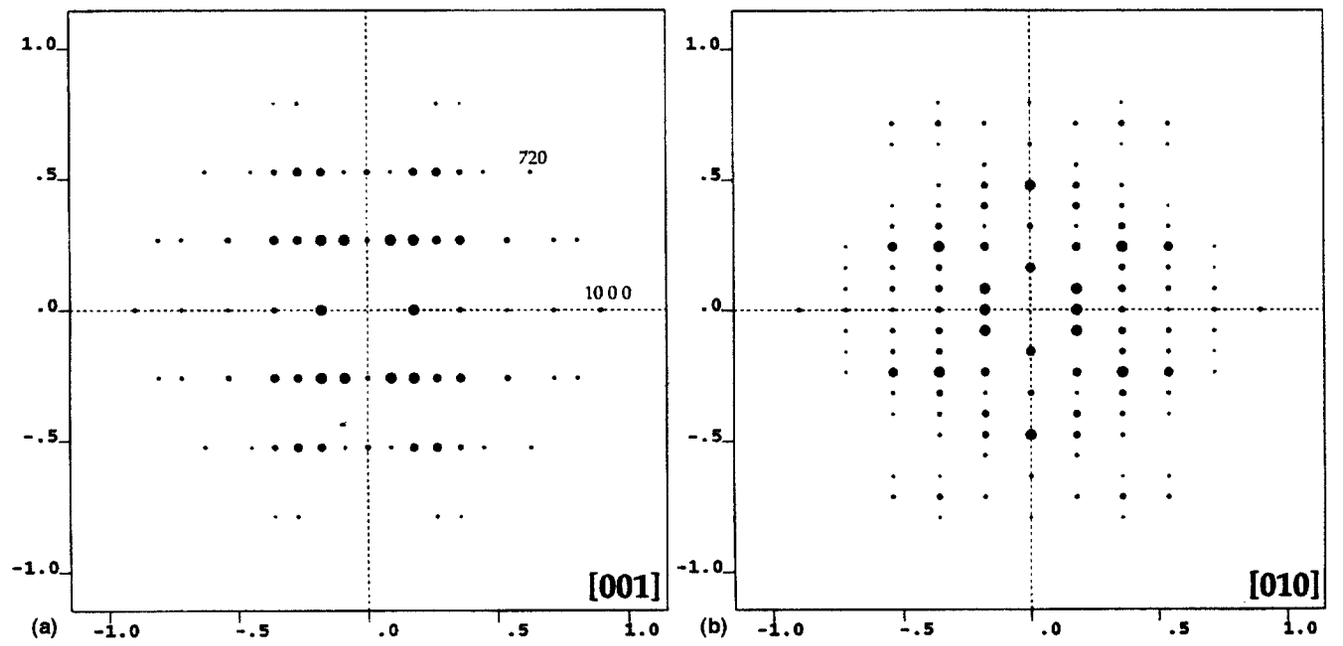

Figure 13 Simulated ED patterns, (a) [001] and (b) [010], based on the cell in *Figure 12a*

The [001] projections of our cell and that of Iannelli and Yoon, which we can approximate using the torsion factor of 0.0, again differ only in the angle between the phenyl ring and the ester group, ours lying closer to parallel (4.3° vs 8.6°, with the ester group plane also being displaced in our cell by a small amount). Calculated ED patterns are shown in *Figure 13* for the two zones of interest relative to *Figure 11*. Other than for the relatively stronger observed {020} and {400} reflections on the [001] pattern, both of which we attribute to secondary scattering from neighbouring strong reflections (110 and 200 for the 020 and 400 reflections), the agreement in intensity distribution is excellent. As in the case of *Figure 5*, the simulated pattern has been printed with a 'high incident intensity' to permit observation of the high order reflections; the relative predicted intensities of 110 and 210, in particular, are incorrectly displayed (see *Table 3*). Particularly interesting is the agreement in the observed and calculated intensities of {600}, {800} and {10.0.0}. The strong {10.0.0} is due to the positioning of high electron density at every 0.1 of the *a*-axis when the atomic positions in *Figure 13a* are projected onto the *a*-axis in the diagram.

The fractional atomic coordinates are listed in *Table 2*; successive phenyl rings lie at an angle of 128° (the same as for the Iannelli and Yoon model) and have the same

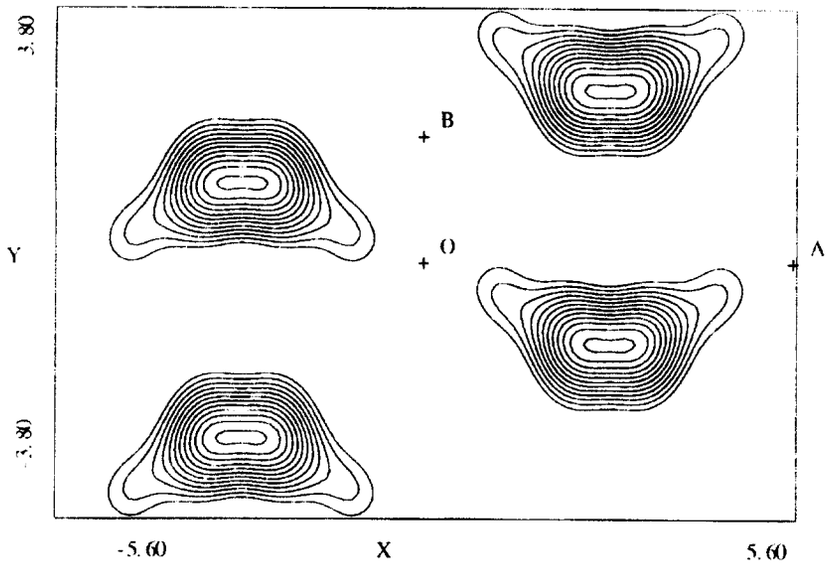

Figure 14 [001] potential map obtained using direct phasing and a pattern similar to that in *Figure 12a*

Table 2 Atomic positions in PpOBA phase I and II crystals

Atom	*x*	*y z*	Atom	*x*	*y*	*z*	
Phase I							
O_1	0.221	0.691	0.043	C_6	0.174	0.638	0.370
O_2	0.362	−0.044	0.064	C_7	0.188	0.656	0.260
O_3	0.221	0.816	0.542	C_8	0.285	0.638	0.604
O_4	0.362	0.465	0.565	C_9	0.266	0.654	0.714
C_1	0.285	0.869	0.103	C_{10}	0.330	0.472	0.778
C_2	0.266	0.855	0.214	C_{11}	0.318	0.489	0.889
C_3	0.330	−0.035	0.278	C_{12}	0.239	0.686	0.935
C_4	0.318	−0.018	0.388	C_{13}	0.174	0.869	0.870
C_5	0.239	0.821	0.435	C_{14}	0.188	0.853	0.759
Phase II							
O_1	0.217	0.187	0.055	C_4	0.386	0.366	0.400
O_2	0.394	0.468	0.077	C_5	0.287	0.213	0.447
C_1	0.306	0.311	0.117	C_6	0.194	0.087	0.384
C_2	0.300	0.271	0.226	C_7	0.201	0.116	0.274
C_3	0.393	0.395	0.290				

Table 3 Structure factors of Pp0BA phase II crystals

hkl	$\lvert F_0\rvert$	'I&Y' $\lvert F_c\rvert$	Our $\lvert F_c\rvert$	*hkl*	$\lvert F_0\rvert$	'I&Y' $\lvert F_c\rvert$	Our $\lvert F_c\rvert$
100	1.58	0.03	0.00	410	9.43	9.51	8.83
200	32.91	35.14	33.51	510	0.29	0.91	0.31
300	2.60	0.02	0.03	610	2.39	2.55	3.44
400	5.88	3.64	3.66	710	1.35	0.67	0.64
600	2.03	0.97	1.23	810	1.06	2.46	2.31
800	1.71	0.59	1.66	910	1.45	1.84	2.38
1000	3.63	2.98	3.63	020	5.05	0.95	2.62
010	5.68	5.57	3.68	120	1.84	2.01	1.53
110	37.30	35.63	37.29	220	6.97	6.47	6.97
210	14.41	11.07	12.80	320	7.23	6.05	7.78
310	11.50	10.71	8.45	420	1.72	5.26	4.31

R-Factors; 'Iannelli & Yoon', 0.191; Our, 0.158

face-to-edge packing as in phase I. A comparison of calculated and observed [001] zone structure factors is given in *Table 3*; an *R*-factor of 0.16 is obtained for a total of 22 independent reflections as compared to a value of 0.19 for our simulation of the Iannelli and Yoon cell. The packing energy for our model was $-178.1\,\text{kcal mol}^{-1}$.

The direct phasing [001] potential map for phase II, based on a pattern similar to that in *Figure 11a*, is shown in *Figure 14*. Comparison with the [001] projection in *Figure 12*, at the current resolution, shows reasonable agreement. The diagram can be interpreted in terms of the phenyl ring angle being *ca* 120°, with the carbonyl oxygen being displaced from the plane of the phenyl ring by *ca* 25°. Being in projection, with numerous overlapping atoms, the [001] potential map for even a polymer with as many reflections as here, will not likely resolve individual atoms.

No staggering is proposed for the molecular packing. However, the streaking of the reflections on the {003}, {006} and {009} layer lines suggests the presence of some disorder in the packing along *c*, possibly some reversed chains and/or a staggering. With only the one relatively good phase II whisker pattern and the central reflections on that ({100} and {111}) being obscured by the main beam, direct phasing was not attempted.

In order to compare our results with the unit cells proposed by Lukasheva *et al.*[17], simulations were done of both *cis*- and *trans*-conformation cells related to those they proposed. Packing energies for many of the cells were similar, in the range of −170 to $-180\,\text{kcal mol}^{-1}$. However, none of the cells yield appropriate ED patterns when both [001] and [100] zones are considered. Although the similarities in packing energies may suggest, as pointed out by Lukasheva *et al.*[17], the likelihood of polymorphism, the observed ED patterns do not indicate that it occurs either in separate crystals or as domains in a single crystal.

X-ray diffraction

X-ray diffraction scans of bulk solution polymerized material, as-polymerized, are shown in *Figure 15***a**. From the bottom the scans are from 300°C, concentrated Marlotherm S solution (14%) polymerized material (i.e. disc-type material) polymerized (a) 13 min and (b) 3 h, respectively, and whiskers polymerized (c) 90 and (d) 5 min at 350°C in a 2% Therminol 66 solution. Note that the order of time of polymerization is reversed to prevent overlap of the scans. As shown by the ratios of the 110(I)/200(II) peaks, the disk material is a mixture of the two phases, increasing in phase II with polymerization time,

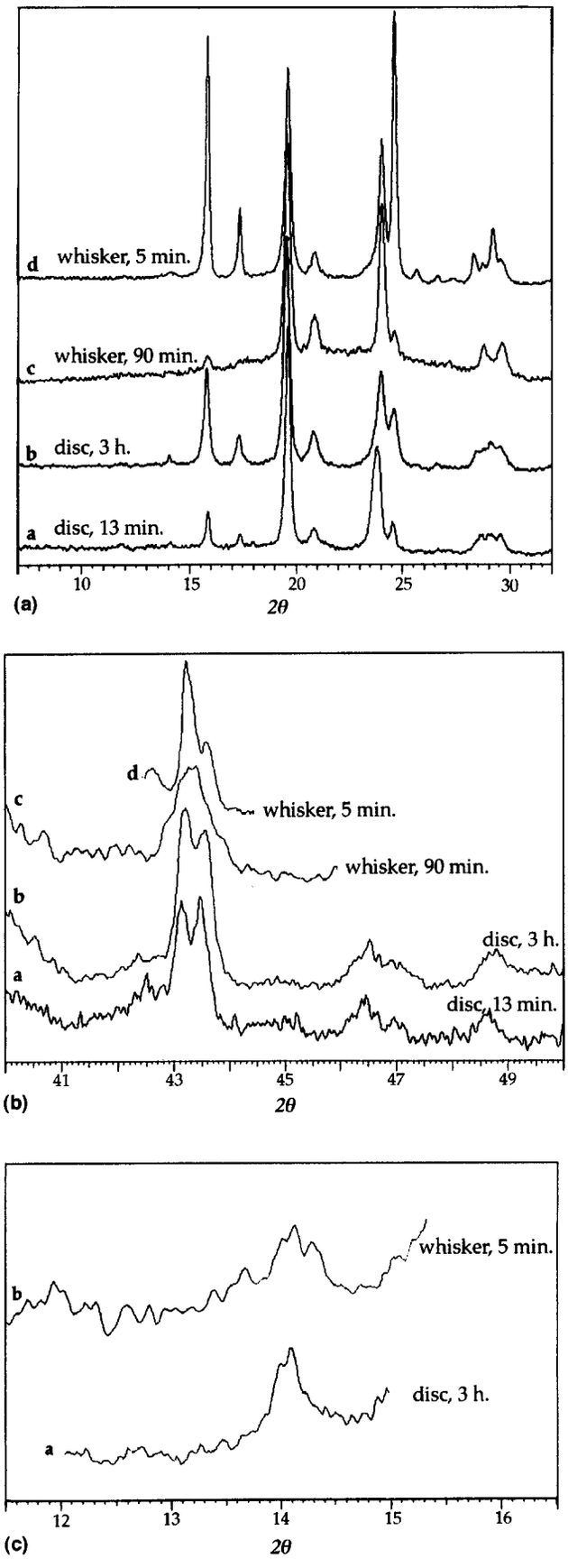

Figure 15 (a) X-ray diffraction scans of disc-type material polymerized for (a) 13 min and (b) 3 h, both at 300°C in a 14% Marlotherm S solution, and whisker-type material polymerized for (c) 5 min and (d) 90 min, both at 350°C in a 2% Therminol 66 solution. (b) Enlarged scans of the 006 2θ portions of the top three scans in (a). The bottom scan is from a whisker sample polymerized for a long time (350°C, 90 min, 1% Therminol 66). (c) Enlarged scans of the 002 2θ portions of the scans in (a) for the 3 h disc (a) and 90 min whisker (b) samples

while for the whiskers the trend is in the other direction, becoming essentially pure phase I with increasing time. This can also be seen from the enlarged scans in *Figure 15***b**, which show the region of the 006 reflections. As pointed out by Iannelli and Yoon[16], 006(II) is at a slightly smaller angle than 006(I); calculated angles based on our values of c are $2\theta = 43.2$ and 43.5°. These peaks are clearly resolved, and of near equal height, in the disc material in the bottom two scans, from the same samples as the bottom two scans in *Figure 15***a**, whereas in the whisker material a double peak is seen for the 5 min polymerized material (d) but only a single, broadened peak is seen centered between the two 006 peaks for a sample similar to that in scan (c) in *Figure 15***a**. The sample in scan (c) in *Figure 15***b** is from a sample polymerized 90 min at 350°C, but with a concentration of 1%. The corresponding 002 peaks would be near 14°; i.e. at 14.1°(II) and 14.2°(I). This region is shown in *Figure 15***c** (bottom, scan (a)) for the 3 h disc-type material in *Figure 15***a**. A doublet would seem to be present, with each peak at an angle 0.1° too small; on the other hand there may be only a single peak present, at the position of 002(II) with the low angle shoulder being noise. The latter would be in agreement with the observations of Iannelli and Yoon; they indicate 002(II) only is visible[16]. The scan from the 90 min whisker sample in *Figure 15***a**, which consists almost entirely of phase I PpOBA, showed no sign of either 002 reflection (not shown in *Figure 15***c**). The scan (*Figure 15***c**, top scan (b)) from the 5 min polymerized sample in *Figure 15***a**, however, containing both phase I and II, again can be interpreted as a double peak at 14.13 and 14.28°. For both 006(II) and 002(II), the streaks parallel to the layer lines observed in the ED patterns will contribute to a broadening of the peaks. Further examination of the low, high and intermediate angle scans of the solution polymerized material as a function of polymerization time, temperature and concentration will be described elsewhere[32].

Simulated X-ray patterns for the cells in *Figures 3*, *4*, and *8* (all phase I) are shown in *Figure 16***a** with phase II simulated patterns from our cell and our model of the Iannelli and Yoon phase II cell in *Figure 16***b**. The simulated scans for the cells in *Figures 3* and *4* are nearly superimposable, with the major differences being slightly different 110/200 and 110/111 phase I peak ratios. These ratios for the 'Iannelli and Yoon' cell are nearly identical to those shown in their paper[16], suggesting our simulated model is very close to theirs. In the whisker scans in *Figure 15***a**, the values of these ratios (3/2) are closer to those for our cell (4/3) than for the Iannelli and Yoon cell (2/1), whereas in their scan from the Polysciences material the ratio is *ca* 2/1. In the disc scans the ratio is even greater than 2/1; it is noted phase II makes a minimal contribution to these reflections, no phase II reflection corresponding in position to 110(I) and 200(I) being at almost the same angle as 010(II), the (minimal) intensity of which should add to that of 200(I) in the disc scans. The intensity of 211 in the simulation in *Figure 16***a** (top) is too large relative to the observed; reducing the crystal size in the c-axis direction from 500 to 150 Å or increasing the lattice strain from 0 to 1% reduces the height (and broadens) 211 to the same height as 210.

The simulated scan for our phase II is also very similar to that of Iannelli and Yoon, the major difference being

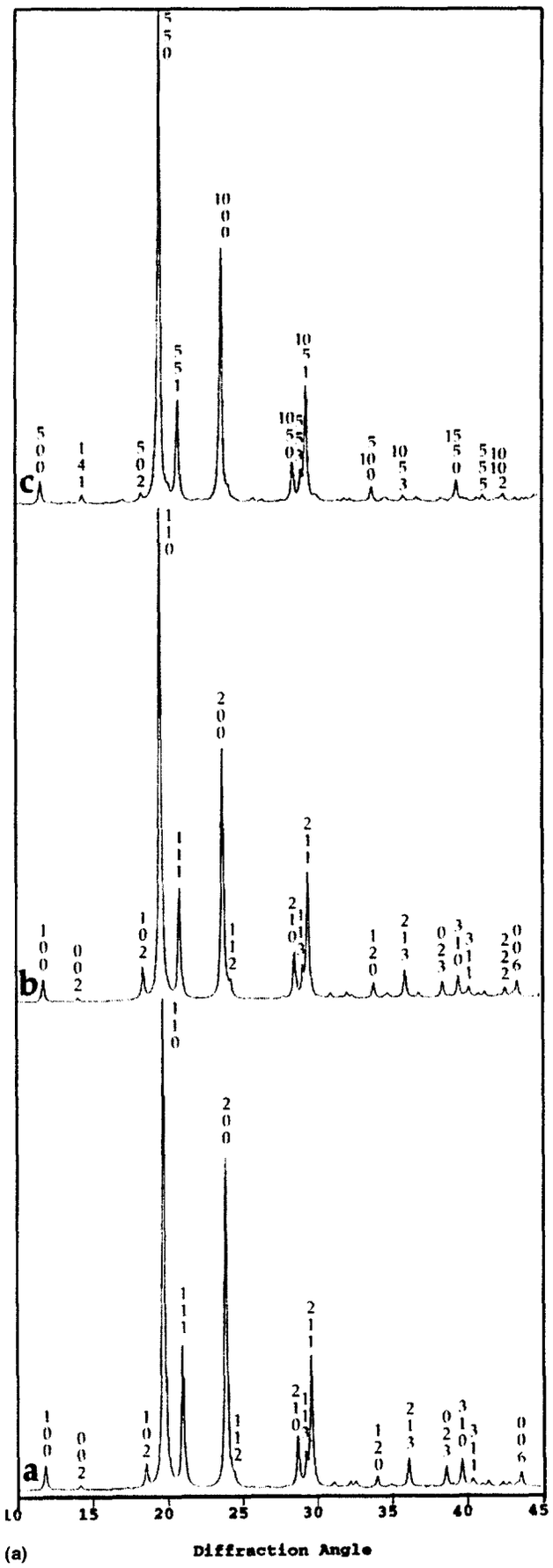

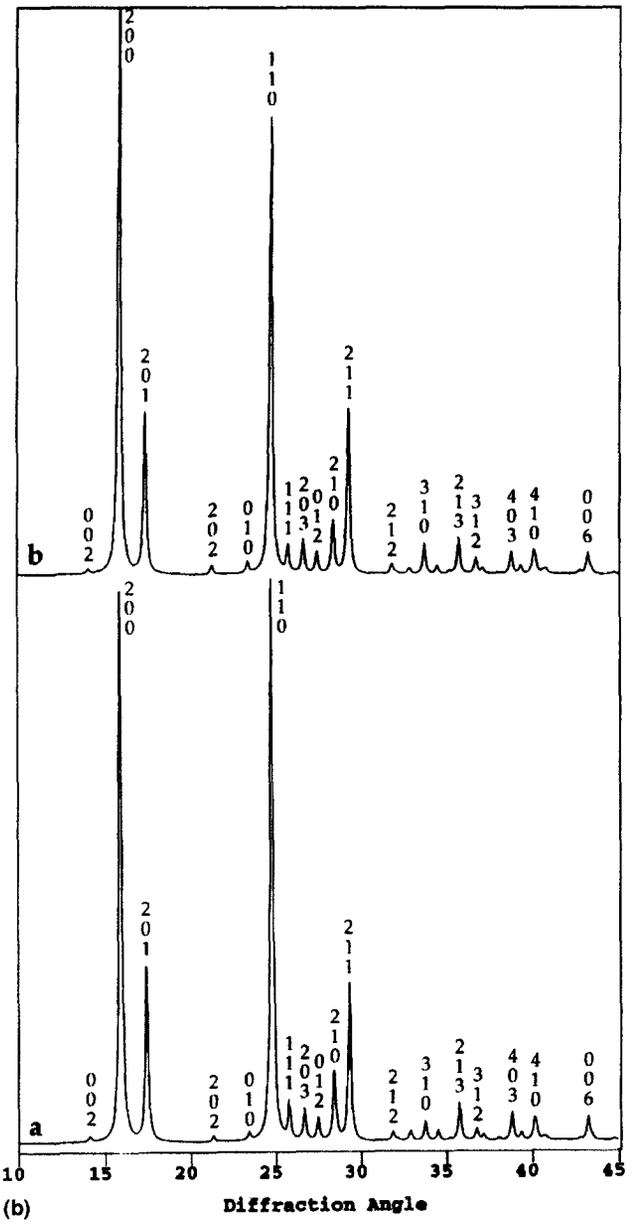

Figure 16 Simulated X-ray powder patterns for (**a**) the phase I cells in *Figures 3*, *4*, and *8*; (**b**) the phase II cell in *Figure 12* and a cell similar to that proposed by Iannelli and Yoon[16] for phase II

an inversion of the ratio of the 200(II)/110(II) intensities from 5/4 in their calculated phase II cell to 17/20 for our cell. In the scan in *Figure 15***a** from the early stage whisker material the ratio is close to that we predict while in the 300 min disc material scan this ratio is *ca* 2/1, in rather poor agreement with both simulations. X-ray scans were also simulated for all of the cells described in relation to *Figures 7*, and the models of Lukasheva *et al.*[17]; none of them shows even approximate agreement with the observed.

006 is seen to be a fairly strong reflection in both phases, while 002 is weak, but present, in all of the simulations in *Figure 16* except that for the scan from the cell in *Figure 8* (*Figure 16***a**, top (c)). The 50/50 random up-down orientation of the molecules, as shown in *Figure 8*, results, in agreement with Iannelli and Yoon[16], in the loss of the 002(I) reflection. The 141 reflection in this pattern is due to the finite size of the superlattice cell chosen; all values of h and k in this pattern need to be divided by five, to compare with the other simulations. The relative strength of 002 in the ED patterns is attributed to the differences in the C and O atomic scattering factors for X-rays and electrons. A similar effect was noted a number of years ago for ED patterns from oriented polyoxymethylene, the 009 and 0018 reflections being present in tilted X-ray fibre patterns but only the 0018 reflection being present in the ED pattern[33]; since O and C have nearly the same electron scattering factors, ED considers the 9/5 helix to be an 18/5 helix. The 002 reflection is present in the simulated [100] ED pattern from the model in *Figure 8*, although reduced in intensity.

DISCUSSION

Two factors of major concern are whether the crystal structure in the lamellae and the whiskers is the same, a factor related to the second, namely whether the molecular weight in either (and both) of our samples is sufficient to consider the material to be polymer rather than oligomer with the chain ends affecting the packing. In addition we consider possible reasons for the difference in our results for Phase I and those of Iannelli and Yoon.

Consider first the molecular weight; the T_{k-m} of the whisker material used here was >350°C. We still have not been able to explain the 20–30°C increase in T_{k-m} of the whiskers over that of the long time polymerized disc material[19,24]. It cannot be attributed to crystal size, for instance, since the lateral size of the whisker crystals is less than that of the disc crystals while the thickness parallel to the molecular axis is extremely large by polymer standards for both types of samples. The measured T_{k-m} is above the scale of the T_{k-m} vs molecular weight curve of Economy *et al.*[3]. Infra-red shows a total loss of the carboxyl and acetoxy bands in the whiskers for long polymerization times, also indicating a high molecular weight. On the other hand, the CTFMP crystals likely have a DP corresponding to extended chains, i.e. 16 for a 100 Å thick crystal. Since the *hk*0 reflections from the single crystals and those that can be measured from the whiskers have the same spacings, we believe the lattice is unaffected by the low DP and is the same in both types of samples.

We attribute the difference between our results and those of Iannelli and Yoon[16], for Phase I, involving the difference in ester group angle with respect to the phenyl rings, the c-axis stagger and the parallel rather than statistical alignment of the molecules, to the difference in type of samples. As in the case of our use of CTFMP crystals to determine the 'perfect' crystal structure of PET[29], we suggest the crystals used here should also be considered 'perfect', being formed by simultaneous polymerization-crystallization even though, for both the disc and whisker crystals, initial growth was likely in the liquid crystal state. The polymerization temperatures used are well above the T_{k-m} for the low molecular weight oligomers proposed[34] to 'crystallize' out as they grow in the solution. On the other hand the thermal history of the samples of Iannelli and Yoon was not given; while simple melting and recrystallization would not be expected to result in randomization of neighbouring molecules in a crystal (transesterification, to which randomization of sequence distribution in related copolymers has been attributed[35] will not result in a reversal of chain direction), melting plus some form of deformation could. For instance, annealing of the CTFMP crystals above T_{k-m} yields complex, twinned single crystal [001] (I) and (II) patterns, but still with many orders[19] whereas shearing of a CTFMP sample above T_{k-m} results in loss of many of the equatorial *hk*0 reflections, as well as to the development of layer line streaks associated with the 002 and 006 reflections[22]. Assuming these as-polymerized samples at least approach crystal perfection, we can only conclude the molecular mechanics unit cell predictions of Lukasheva *et al.*[17], particularly for Phase I, are incorrect. We also suggest such predictions should include predictions (simulations) of the corresponding diffraction patterns, permitting immediate comparison with experiment.

CONCLUSIONS

1. The use of CTFMP and/or solution polymerized-crystallized lamellar crystals has permitted the obtaining of high order *hk*0 ED patterns for PpOBA. Although the limiting cone of diffraction imposed by the restriction on mechanical tilting of the sample in the TEM could be overcome by shearing of the sample above T_{k-m}, yielding fibre ED patterns, considerably better, single crystal patterns were obtained using solution grown whiskers. With Kricheldorf and his group having polymerized a large number of condensation homo- and co-polymer whiskers[36], the use of whiskers to overcome the cone of reflection problem adds another tool for this purpose to epitaxial crystallization and shearing[25], increasing the potential of ED for full polymer crystal structure determination. It is suggested the patterns obtained from the as-polymerized samples represent 'perfect' crystals, i.e. ones in which processing induced defects such as statistical chain directions, intra-crystal chain ends, *cis–trans* isomerization, etc. are minimal.
2. Least squares refinement of the unit cell parameters yield the values in the abstract for the two phases, I and II. These values are nearly the same as those proposed recently by Iannelli and Yoon based on X-ray powder diffraction patterns[16].
3. Modelling of the unit cells using the Cerius[2] software suggests a *cis*-conformation for the chains in both phases, with the chains in the phase I cell being

staggered by ±0.14 Å along the *c*-axis. As a result of the stagger, the phase I space group is triclinic (metrically orthorhombic, $\alpha = \beta = \gamma = 90°$) *P*1, rather than the $Pbc2_1$ orthorhombic cell proposed by Iannelli and Yoon[16]. The phase II space group is $Pca2_1$ with only slight differences with the cell of Iannelli and Yoon proposed; streaking of some of the reflections from the whisker suggests axial disorder. For both cells a parallel packing of the chains is proposed. It is emphasized that the differences between our cells and those proposed by Iannelli and Yoon are believed due to differences in sample history; we suggest nascent crystalline polymers will often have a more 'perfect' crystal structure than after any processing history.

4. Initial results of direct phasing yield electrostatic potential maps in good, but not perfect, agreement with the Cerius[2] models. Further studies in this area are in progress, with particular concern for the effects of multiple scattering on both types of modelling and the assumption of a 2_1 screw along *c* for the direct phasing of the whisker pattern. The direct phasing, in particular, confirms the molecular stagger along the *c*-axis in the phase I cell in the whiskers.
5. Comparison of the simulated X-ray patterns, amongst themselves and with the observed patterns, taking into consideration the effect of crystal size and lattice strain, indicates the difficulty of X-ray diffraction characterization of polymer crystal structures, even of nascent polymers. On the other hand, we recognize the potential problems of beam damage, multiple scattering and intensity measurement, as well as low molecular weight, in our use of ED for the characterization.

ACKNOWLEDGEMENTS

This research was supported, in part, by the National Science Foundation through grants 93-12823 (J. L., P. H. G.), 89-20538 (B. -L. Y.) and 94-17835 (D. L. D.).

REFERENCES

1. Economy, J., Storm. R. S., Matkovic, V. I., Cottis, S. G. and Novak, B. E., *J. Polym. Sci., Polym. Chem. Edn*, 1976, **14**, 2207.
2. Yoon, D. Y., Masciocchi, N., Depero, L. E., Viney, C. and Parrish, W., *Macromolecules*, 1990, **23**, 1793.
3. Economy, J., Volksen, W., Viney, C., Geiss, R., Siemans, R. and Karis, T., *Macromolecules*, 1988, **21**, 277.
4. Lieser, G., *J. Polym. Sci., Polym. Phys. Edn*, 1983, **21**, 1611.
5. Tadokoro, H., in *Structure of Crystalline Polymers*. Wiley, New York, 1979.
6. Geiss, R., Street, B., Volksen, W. and Economy, J., *IBM J. Res. Dev.*, 1983, **27**, 321.
7. Economy, J., Volksen, W. and Geiss, R., *Mol. Cryst. Liq. Cryst.*, 1984, **105**, 289.
8. Biswas, A. and Blackwell, J., *Macromolecules*, 1988, **21**, 3158.
9. Hasegawa, R. K., Chatani, Y. and Tadokoro, H., presented at a meeting of the Crystallographic Society of Japan, Osaka, 1973, p. 21.
10. Tashiro, K., Kobayshi, M. and Takayanagi, M., *Macromolecules*, 1977, **10**, 413.
11. Northolt, M. G. and van Artsen, J. J., *J. Polym. Sci., Polym. Letts Edn*, 1973, **11**, 333.
12. Coulter, P. D., Hanna, S. and Windle, A. H., *Liq. Cryst.*, 1989, **5**, 1603.
13. Coulter, P. D., and Windle, A. H., *Macromolecules*, 1989, **22**, 1129.
14. Sun, Z., Cheng, H.-M. and Blackwell, J., *Macromolecules*, 1991, **24**, 4162.
15. Iannelli, P., Yoon, D. Y. and Parrish, W., *Macromolecules*, 1994, **27**, 3295.
16. Iannelli, P. and Yoon, D. Y., *J. Polym. Sci., Polym. Phys.*, 1995, **33**, 977.
17. Lukasheva, N V., Mosell, T., Sariban, A. and Brickmann, J., *Macromolecules*, 1996, **29**, 1286.
18. Liu, J. and Geil, P. H., *J. Macromol. Sci., Phys.*, 1992, **B31**, 163.
19. Liu, J., Rybnikar, F. and Geil, P. H., *J. Macromol. Sci., Phys.*, 1993, **B33** 395.
20. Liu, J. and Geil, P. H., *Polymer*, 1993, **34**, 1366.
21. Liu, J. and Geil, P. H., *Macromol. Rpts*, 1993, **A30**, 183.
22. Rybnikar, F., Liu, J. and Geil, P. H., *Macromol. Chem. Phys.*, 1994, **195**, 81.
23. Rybnikar, F., Yuan, B.-L. and Geil, P. H., *Polymer*, 1994, **35**, 1863.
24. Yuan, B. -L., Liu, J., Geil, P. H., Tappin, K., Robertson, I., Patel, D. and Bassett, D. C., paper presented at American Physical Society meeting, March, 1994, Pittsburg, PA (to be published).
25. Dorset, D. L., *Structural Electron Crystallography*. Plenum, New York, 1995.
26. Voight-Marten, I. G., Yan, D. H., Gilmore, C. J., Shankland, K. and Bricogne, G., *Ultramicroscopy*, 1994, **56**, 271.
27. Dorset, D. L. and McCourt, M. P., *Acta Cryst.*, 1994, **A50**, 287.
28. Vainshtein, B. K. and Lobachev, A. N., *Sov. Phys. Crystallogr.*, 1995, **1**, 370.
29. Liu, J. and Geil, P. H., *J. Macromol. Sci., Phys.*, 1997, **B36**, 263.
30. Liu, J. and Geil, P. H., *J. Macromol. Sci., Phys.*, 1997, **B36**, 61.
31. Liu, J., Long, T.-C., Geil, P. H. and Rybnikar, F., *J. Polym. Sci., Polym. Phys.*, 1996, **34**, 2843.
32. Yuan, B.-L., Ph.D. thesis, University of Illinois at Urbane-Champaign, in preparation.
33. O'Leary, K. and Geil, P. H., *Makromol. Chem.*, 1968, **118**, 77.
34. Kricheldorf, H., Schwarz, G. and Lieser, G., *J. Polym. Sci., Polym. Phys. Edn*, 1983, **21**, 1599.
35. Economy, J. and Goranov, K., in *High Performance Polymers*, Advances in Polymer Science, Vol. 117. Springer-Verlag, Berlin, 1994.
36. Schwarz, G. and Kricheldorf, H. R., *Macromolecules*, 1995, **28**, 3911.